Available online at www.sciencedirect.com
SCIENCE DIRECT®
Journal of Power Sources 146 (2005) 146–150
JOURNAL OF POWER SOURCES
www.elsevier.com/locate/jpowsour

Capacity fading of lithiated graphite electrodes studied by a combination of electroanalytical methods, Raman spectroscopy and SEM

E. Markervich, G. Salitra, M.D. Levi, D. Aurbach *

Department of Chemistry, Bar-Ilan University, 52900 Ramat-Gan, Israel

Available online 25 April 2005

Abstract

We present herein Raman spectroscopy and SEM characterizations of composite graphite electrodes in conjunction with classical electroanalytical characterizations (SSCV and EIS) during prolonged cycling. During cycling, graphite particles crack into smaller pieces that are less oriented than the original platelets, with the possible filling of the cracks thus formed by the reduction products of the electrolyte solution. In addition, the average crystalline size (estimated by Raman spectroscopy) decreases as cycling progresses. The borders between the crystallites may possess dangling bonds and generally contain low-energy (or hollow) sites for irreversible interaction with Li-ions and solution species. The redistribution between the hollow and the shallow sites (i.e. the site for reversible Li-ion storage) occurring during electrode cycling is responsible for the moderate decrease of the reversible capacity of graphite electrodes observed during prolonged cycling.

Keywords: Li-ion batteries; Graphite anode; Capacity fading; Raman spectroscopy; SEM imaging; Crystal structure

1. Introduction

The capacity fading of Li insertion electrodes and its possible mechanisms are very important issues in the study of Li-ion battery systems and their components.

Understanding capacity fading processes is a prerequisite to any prediction of calendar life and long-term performance of Li-ion batteries [1–3]. It is known that charged electrodes (lithiated graphite, delithiated Li_xMO_2 transition metal oxides) may undergo self-discharge that may be partially reversible, but are mostly irreversible [4]. The self-discharge of graphite electrodes may be quantified using the self-discharge current, which may be calculated from OCV measurements of fully charged (lithiated) electrodes:

$$I_{sd} = \frac{dE}{dt}\frac{dQ}{dE},$$

where dE/dt is measured at open circuit conditions and dQ/dE is calculated from the dependence of the intercalation capacity on the electrode's potential (e.g. obtained by slow scan rate CV) [5].

In a recent paper [6], we presented in detail the results of slow scan rate cyclic voltammetry (SSCV), electrochemical impedance (EIS) and differential self-discharge studies of composite graphite electrodes as a function of the cycle number during 140 cycles. There is an interesting correlation between the dependence of the rate of self-discharge and the impedance of the electrodes in the fully intercalated and deintercalated states on the cycle number. This correlation could be explained in terms of the formation, growing, reformation and densification of the surface films surrounding the graphite particles (the rate of S.D. decreases during the first 40 cycles and so does the high-frequency impedance). The turning point is observed after about 40 cycles, after which the rate of the S.D. sharply increases because of a gradual deterioration of the insulating properties of the surface films (structural defects are accumulated

* Corresponding author. Tel.: +972 3 531 8317; fax: +972 3 535 1250.
E-mail address: aurbach@mail.biu.ac.il (D. Aurbach).

0378-7753/$ – see front matter © 2005 Elsevier B.V. All rights reserved.
doi:10.1016/j.jpowsour.2005.03.107

during cycling). However, the total charge capacity of the electrode showed a very slow, gradual decrease during cycling.

In order to understand the reasons for the capacity fading of graphite electrodes when cycled at ambient temperature, we supplemented the electroanalytical studies with Raman spectroscopy and SEM characterizations, which could shed light on the correlation between the properties of the surface films, the high-frequency impedance and the reversible capacity.

2. Experimental

The preparation of thin composite graphite electrodes has been described previously [7–9]. The electrode usually contained 1.4 mg of graphite powder (KS-15 from Timrex Inc.) and 10 wt% of PVdF binder. The cell was a standard 2032 coin-type cell (NRC, Canada), containing a composite graphite working electrode (with a geometric surface area of 1.5 cm^2) and Li counter and reference electrodes. The cell was hermetically sealed by a standard crimping device and additionally isolated with epoxy glue (for details, see Ref. [10]). The cell was operated at $25 \pm 0.1\,^{\circ}C$. The electrolyte solution was 1 M $LiPF_6$ in an ethylene carbonate (EC) + dimethylcarbonate (DMC) 1:1 mixture (Li-battery grade from Merck, KGaA).

The initial surface film formation was performed by galvanostatic polarization of a fresh graphite electrode in the potential range of 2.5 V (OCV) to 0.3 V. Thereafter, a slow scan rate (10 $\mu V\,s^{-1}$) potentiodynamic sweep from 0.3 to 0.03 V was applied, followed by potentiostatic polarization at this potential to fully complete the Li insertion into LiC_6. The impedance of the fully lithiated electrodes was then measured, after which the anodic branch of the SSCV was measured at the same scan rate while sweeping the potential up to 0.3 V. This set of measurements was repeated for each of a total 140 cycles.

Fast and slow scan rate CV and EIS techniques were applied using a computerized potentiostat–galvanostat Model 20 Autolab, from Eco Chemie Inc., which included a FRA module. The collection of data was controlled by the GPES Version 4.9 Eco Chemie B.V. Software (Utrecht, The Netherlands).

Raman spectra of graphite electrodes were measured ex situ in a back-scattered configuration through the optical glass in a hermetically closed cell, using a micro-Raman spectrometer HR800 (Jobin Yvon Horiba), holographic grating 1800 grooves mm^{-1}, with an Ar-laser (excitation line 514.5 nm, 0.2 mW), objective 50× (numerical aperture 0.75). The morphology of the electrodes was examined by a SEM (JEOL-JSM 840 microscope).

3. Results and discussion

3.1. Electroanalytical study of the long-term cycling of a graphite electrode

Fig. 1 summarizes our previous findings [6] concerning the unusual correlation between the moderate decrease in reversible capacity during electrode charge with the cycle number, and the parallel decrease (followed by stabilization) of the high-frequency impedance of the same electrode measured in the fully intercalated state at 0.03 V. The commonly accepted reasons for the capacity fading of composite graphite electrodes in Li-ion cells include: (i) The growth of electronically insulating surface films, which causes a slow down of the kinetics, and eventually leads to the electrical disconnection of an increasing fraction of the graphite particles from the current collector [11–13]. (ii) Depletion of the electrolyte solution due to continuous surface reactions. Solution depletion relates, of course, to prolonged cycling and to elevated temperatures [14]. (iii) The exfoliation of the graphene planes [15]. During cycling of the cell at ambient temperature, we observed quite different trends, basically incompatible with

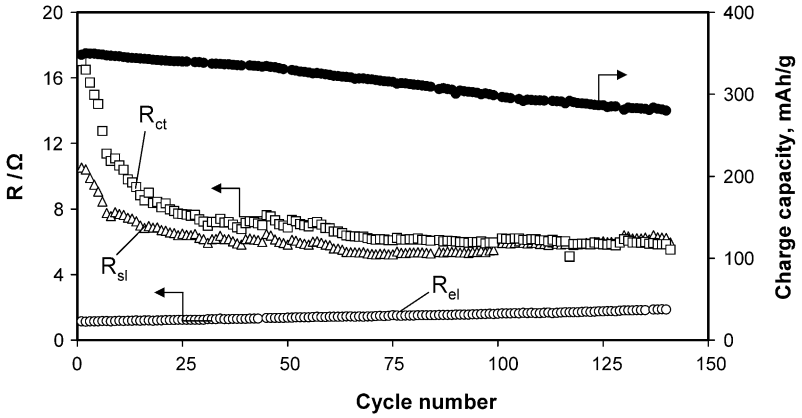

Fig. 1. Total charge capacity and three resistances, R_{el}, R_{sl} and R_{ct}, measured at 0.03 V as functions of the cycle number of a graphite electrode cycled potentiodynamically with a scan rate of 10 $\mu V\,s^{-1}$ in 1 M $LiPF_6$ in an EC:EMC 1:2 electrolyte solution at 25 °C.

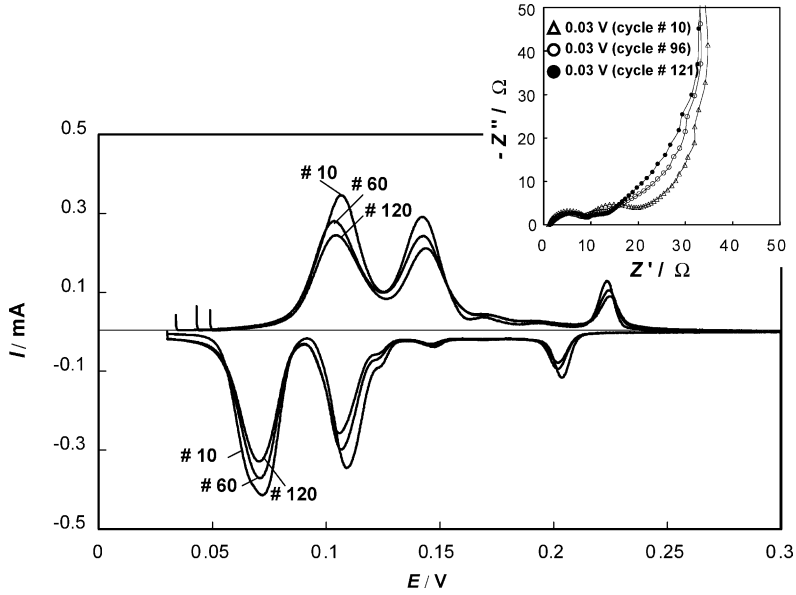

Fig. 2. Slow scan rate potentiodynamic scans ($\nu = 10\ \mu V\ s^{-1}$) for Li-ion insertion and deinsertion into/from a composite graphite electrode, cycles #10, 60 and 120 as indicated. The active graphite mass was 1.4 mg. Electrolyte solution composition: 1 M $LiPF_6$ in EC:EMC 1:2 at 25 °C. The inset in Fig. 2 shows a family of impedance spectra for the fully lithiated graphite electrode ($E = 0.03$ V) during the cycle life of the electrode (cycles #10, 96 and 121).

the above first two reasons: the surface layer resistance R_{sl} at 0.03 V decreases from cycle to cycle (Fig. 1). The shape of the CV curves is also consistent with these data (Fig. 2), as they show very similar voltammograms in term of kinetic parameters, such as peak width and hysteresis. The CVs in Fig. 2 reflect some loss of the active mass upon cycling, but the limitation due to the slow kinetics is not pronounced. The electrolyte resistance R_{el} increases only moderately.

One can propose that the loss of active mass during prolonged cycling relates to the internal graphite structure degradation, which occurs during repeated lithium ion insertion–deinsertion cycles. To investigate changes in the structure of the graphite electrode, Raman spectroscopy and imaging by scanning electron microscopy (SEM) were used.

3.2. The Raman spectroscopy study of a graphite electrode microstructure

Raman spectroscopy is an appropriate method for studying the microstructure of a variety of carbonaceous materials (including graphite) [16–22]. The first-order Raman spectrum of highly crystalline graphite consists of a sharp band at 1580 cm^{-1} (E_{2g2} mode), known as the G band, associated with in-plane symmetric C–C stretches. Polycrystalline graphite and disordered carbons exhibit an additional peak at about 1350 cm^{-1} (A_{1g} mode, D band), which is induced due to the disorder associated with finite crystallites sizes. The ratio $R = I_D/I_G$ of the integrated intensity of the disorder-induced peak at 1350 cm^{-1} to that of the graphite peak at

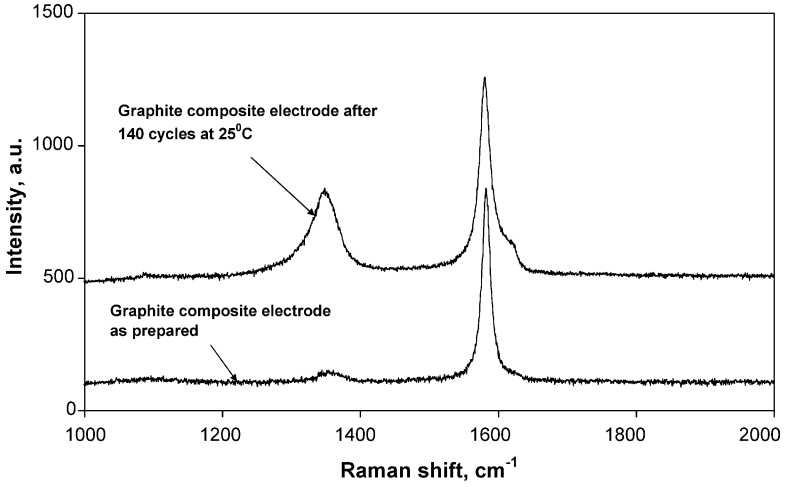

Fig. 3. Raman spectra of a pristine composite graphite electrode and the same electrode after 140 potentiodynamic intercalation–deintercalation cycles ($10\ \mu V\ s^{-1}$) in a 1 M $LiPF_6$ in EC:EMC 1:2 electrolyte solution at 25 °C.

1580 cm^{-1} is generally used to characterize the degree of disorder in carbon materials [D band]. The average in-plane crystallite domain size L_a (Å) can be estimated using Eq. (1) as [16,17,22]:

$$L_a = 44\left(\frac{I_D}{I_G}\right)^{-1}. \quad (1)$$

Fig. 3 displays typical Raman spectra of two graphite electrodes, namely a pristine, as-prepared composite electrode and the same electrode after 140 intercalation–deintercalation cycles at 25 °C (100% depth of discharge). The Raman active E_{2g2} mode vibration peak at 1580 cm^{-1} is the major feature of the pristine electrode spectrum, with the D band appearing relatively weak. Long-term cycling induces a disorder: the D peak grows together with its overtone—a shoulder at 1620 cm^{-1} (band D′). The *R*-values were estimated for the pristine and the cycled electrodes as an average value for six different points on the basal plane surfaces of relatively large graphite flakes. Average value for the pristine electrode was 0.22 ± 0.05, 0.79 ± 0.45 for cycled electrode and the estimated crystalline sizes according to Eq. (1) above were 215 ± 75 and 69 ± 34 Å, respectively. Along with the *R*-ratio, the line width of the G band increased from 15.8 ± 1.2 to 18 ± 1.7 cm^{-1}. This testifies that the long-term repeated lithium intercalation–deintercalation process induces some kind of defects and disorder in the crystal structure of graphite, which result in the decrease of the average crystallite size.

Similar crystal structure changes, detected both by Raman and XRD methods, were reported to occur with graphite electrodes under conditions of mechanic stress [23], irradiation [24], doping [25], etc. An appreciable growth of the *R*-ratio (from 0.042 to 0.333) was observed as well after the first lithium deinsertion from the natural graphite electrode [26]. The decrease of the graphite microcrystal size along the axis *c* (L_c) for natural graphite during the intercalation cycle was demonstrated by XRD measurements as well [27]. Thus, lithium insertion into highly crystalline graphite electrodes produces stress, which leads to structure degradation such as stacking disorder and new boundary formations between newly formed microcrystallites.

3.3. SEM imaging of the electrodes

Fig. 4 shows typical SEM images of the surface morphology of pristine (a) and cycled (b and c: different locations) electrodes. Flat and homogeneous areas of the pristine graphite flakes oriented with their basal planes are clearly seen. The surface of the cycled electrode seems to be different from that of uncycled electrode: cracks appear to be the frequent feature (Fig. 4b), and flakes that are partially exfoliated, forming cavities between the layers, which are probably filled with the electrolyte solution. These cavities are preferred locations for the continuous reduction of solution components. Hence, upon prolonged cycling, they may contain mostly surface species (solution reduction products) (Fig. 4c).

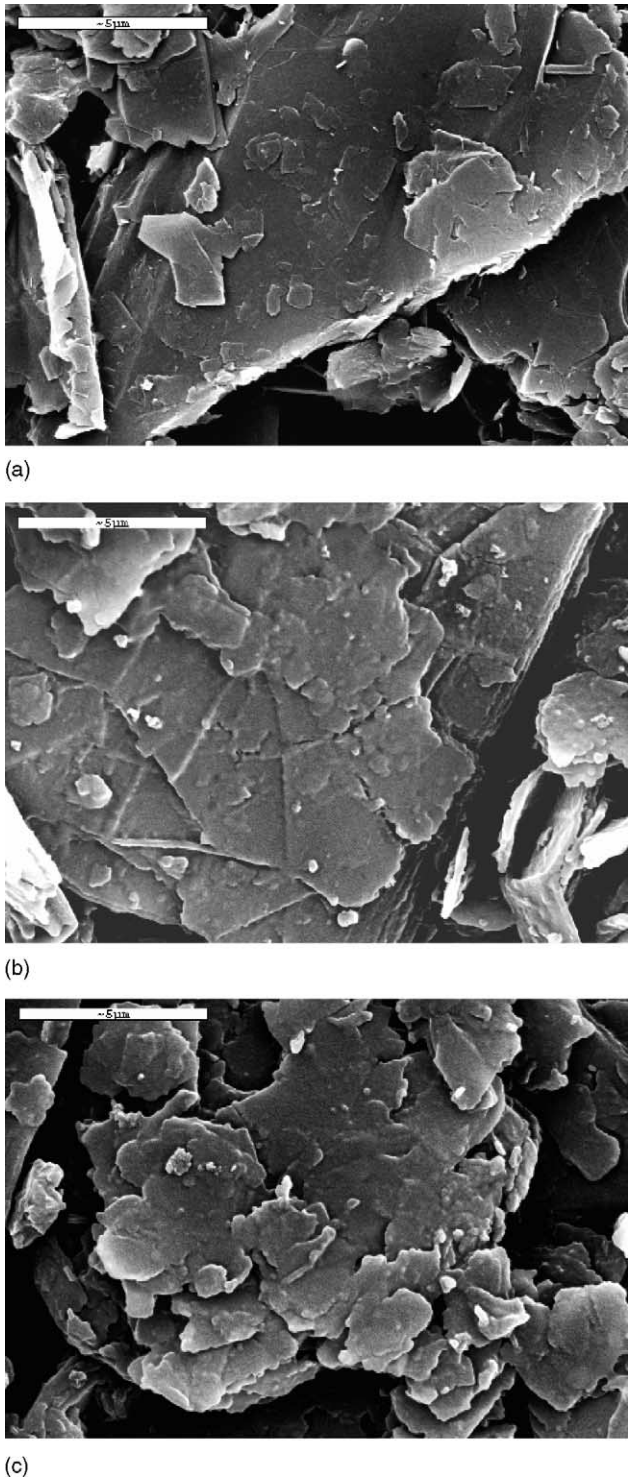

Fig. 4. SEM images of the surface of the KS-15 composite pristine electrode (a) and the same electrode after 140 intercalation–deintercalation cycles at 25 °C (b and c).

Obviously, the average particle size decreases, which is in line with the decrease in the high-frequency impedance (Figs. 1 and 2 (inset)). The increase in the ratio surface

area/volume is also consistent with the model, describing the specific change in the shape of the impedance spectra of the cycled electrode in the medium-frequency domain, namely the development of the low-frequency arc between the middle-frequency (charge transfer) semicircle and the Warburg diffusion domain (see the inset in Fig. 2; more details are reported in Ref. [6]).

Thus, both Raman spectroscopy and SEM imaging converge to prove that during reversible lithium insertion into graphite electrodes substantial mechanical stress develops, which damages the crystal structure of these electrodes both at micro- and nanoscale levels. Such changes offer a probable explanation for the moderate capacity fading during prolonged cycling of composite graphite electrodes at ambient temperatures. One possible reason is the decrease in the number of the sites suitable for reversible lithium ion accommodation, due to the cracking of graphite flakes and the formation of new boundaries between the crystallites, which are not always necessarily accessible to the electrolyte solutions. These boundaries, formed as a result of the long-term cycling of the electrode, may offer sites for irreversible lithium ion storage. “Dangling” bonds, which are formed during crystallite segmentation, may trap lithium ions to form the so-called “strongly bonded” species with a very low potential energy (the hollow sites, in contrast to the shallow sites, in which lithium ions are stored reversibly [28,29]). The appearance of the above hollow sites offers an alternative explanation for the low-frequency arcs in the impedance spectra of cycled electrodes (see the inset in Fig. 2), in addition to the fracturing of the graphite particles, resulting in cracks that become filled with the electrolyte solution (and later may contain solution reduction species). The assumption that composite graphite electrodes may possess several types of intercalation sites within a certain range of energies is in agreement with that of Cazanelli et al. for the graphitized amorphous carbon films [30].

4. Conclusion

Our previous combined differential self-discharge, SSCV and EIS studies of long-term cycled composite graphite electrodes (at room temperature) were supplemented herein by Raman spectroscopy and SEM characterizations of pristine and cycled electrodes. The latter two techniques provide a great deal of evidence that long-term cycling results in two kinds of effects: (i) Primary, graphite platelet particles are fractured to smaller, less-oriented pieces, with possible filling of the cracks formed with the electrolyte solution (together with the reformation and densification of the surface films. This results in a decrease in the high-frequency impedance versus cycle number because of the increase in the surface area of the active mass). (ii) The average crystalline size decreases with the number of cycles (as evidenced from Raman spectroscopy data). The newly formed borders between the crystallites are not necessarily accessible to the electrolyte solution. However, they may possess dangling bonds, and hence, may contain low-energy (or hollow) sites for irreversible storage of Li-ions (disordered carbons present a great deal of evidence for such a mechanism of charge storage). The redistribution between the hollow and the shallow sites (i.e. the site for reversible Li-ions storage) occurring during electrode cycling is responsible for the moderate decrease of the reversible capacity of the electrode.

References

[1] M. Broussely, S. Herreyre, P. Biensan, P. Kasztejna, K. Nechev, R.J. Staniewicz, J. Power Sources 97 (2001) 13.
[2] G. Sarre, P. Blanchard, M. Broussely, J. Power Sources 127 (2004) 65.
[3] H. Ploehn, P. Ramadass, R. White, J. Electrochem. Soc. 151 (2004) A456.
[4] R. Yazami, Y.F. Reynier, Electrochim. Acta 47 (2002) 1217.
[5] M.D. Levi, C. Wang, D. Aurbach, J. Electrochem. Soc. 151 (2004) A781.
[6] M.D. Levi, E. Markevich, D. Aurbach, J. Electrochem. Soc. 152 (2005) A778.
[7] M.D. Levi, D. Aurbach, J. Phys. Chem. B 101 (1997) 4630.
[8] M.D. Levi, D. Aurbach, J. Phys. Chem. B 101 (1997) 4641.
[9] M.D. Levi, D. Aurbach, Electrochim. Acta 45 (1999) 167.
[10] M.D. Levi, C. Wang, J.S. Gnanaraj, D. Aurbach, J. Power Sources 119–121 (2003) 538.
[11] D. Aurbach, J. Power Sources 119 (2003) 497.
[12] D. Aurbach, M.D. Levi, E. Levi, A. Schechter, J. Phys. Chem. B 101 (1997) 2195.
[13] R. Yazami, Electrochim. Acta 45 (1999) 87.
[14] P. Arora, R. White, M. Doyle, J. Electrochem. Soc. 145 (1998) 3647.
[15] M. Winter, J.O. Besenhard, in: J.O. Besenhard (Ed.), Handbook of Battery Materials, Wiley/VCH, Weinheim, 1999, p. 383 (Chapter 5).
[16] F. Tuinstra, J.L. Koenig, J. Chem. Phys. 53 (1970) 1126.
[17] D. Knight, W. White, J. Mater. Res. 4 (1989) 385.
[18] Y. Kawashima, G. Katagiri, Phys. Rev. B 52 (1995) 10053.
[19] J.-C. Panitz, F. Joho, P. Novak, Appl. Spectrosc. 53 (1999) 1188.
[20] J.-C. Panitz, P. Novak, O. Haas, Appl. Spectrosc. 55 (2001) 1131.
[21] O. Beyssac, B. Goffe, J.-P. Petitet, E. Froigneux, M. Moreau, J.-N. Rouzaud, Spectrochim. Acta, Part A 59 (2002) 2267.
[22] H. Wilhelm, M. Lelaurain, E. McRae, B. Humbert, J. Appl. Phys. 84 (1998) 6552.
[23] D. Aurbach, B. Markovsky, A. Nimberger, E. Levi, J. Electrochem. Soc. 149 (2002) A152.
[24] E. Asari, Carbon 38 (2000) 1857.
[25] M. Endo, T. Hayashi, S.-H. Hong, J. Appl. Phys. 90 (2001) 5670.
[26] Q. Pan, K. Guo, L. Wang, S. Fang, J. Mater. Chem. 12 (2002) 1833.
[27] C. Yuqin, L. Hong, W. Lie, L. Tianhong, J. Power Sources 68 (1997) 187.
[28] R. Brittihn, R. Herr, D. Hoge, J. Power Sources 44 (1993) 409.
[29] F. Beguin, F. Chevallier, C. Vix, S. Saadalah, J.N. Rouzaud, F. Frackowiak, J. Phys. Chem. Solids 65 (2004) 211.
[30] E. Cazanelli, G. Mariotto, F. Decker, J.M. Rosolen, J. Appl. Phys. 80 (4) (1996) 2442.